Design and research of an overmoded structure for megawatt-class *Ka*-band extended interaction klystron

Yifan Zu,[1] Xuesong Yuan,[1,a)] Xiaotao Xu,[1] Qingyun Chen,[1] Matthew Cole,[2] Yong Yin,[1] Hailong Li,[1] Bin Wang,[1] Lin Meng,[1] and Yang Yan[1]

AFFILIATIONS

[1]Terahertz Science and Technology Key Laboratory of Sichuan Province, School of Electronic Science and Engineering, University of Electronic Science and Technology of China, Chengdu 610054, China

[2]Department of Electronic and Electrical Engineering, University of Bath, North Road, Bath BA2 7AY, UK

[a)]Author to whom correspondence should be addressed: yuanxs@uestc.edu.cn

ABSTRACT

For most of the applications in the millimeter wave band, corresponding to *Ka* and higher-frequency bands, the relatively high atmospheric absorption necessitates the use of high-power sources. Here, a new approach for projecting an oversized beam tunnel in an overmoded structure by concentrating the axial field is demonstrated to meet the high-frequency and high-power demands of compact devices. Due to the enhanced high-current intense beam loading capability of the interaction circuit, a six-cavity *Ka*-band extended interaction klystron (EIK) with a four-coupling-hole disk-loaded structure is designed that can stably obtain high output power. An analysis of optimization trade-offs from introducing high order modes for allowing the application of more powerful beams to improving high order modes field distribution for enhancing the electron-wave coupling and suppressing mode competition is reported. 3-D particle in cell (PIC) simulations show that such new design approaches can achieve an output power of 1.11 MW at 32.94 GHz with a saturated gain of 57 dB by injecting a 3.3 mm diameter electron beam with a current of 24 A.

I. INTRODUCTION

Advances in microwave and millimeter wave technology are driving the continued development of advanced diagnostic technologies in various fields, such as radio astronomy, biomedical research instruments, high resolution radar, and plasma diagnostics.[1–6] Especially for some applications, there are clear advantages to going up in frequency.[7] When designing next generation acceleration drivers, higher drive frequencies generally allow for higher operating gradients, which will significantly reduce the footprint and construction cost of the accelerator.[8, 9] Millimeter wave band enables radar designers to achieve high energy density and angular resolution in space with practical transmitter power and antenna aperture; employ wide instantaneous bandwidth; and gain increased Doppler frequency shifts for a specified radial velocity spread.[10, 11] The same properties such as high-power density and localization that make millimeter-wave systems attractive in future devices will also enable smaller fusion research devices to play an important role in the development of fusion energy.[12, 13] Progress in these fields is closely related to the development of high-power electronics in the millimeter wave band.

The quest for high peak power has spurred interest in the production of microwave power using relativistic electron beams. However, the practical applicability of short-pulse high-power relativistic devices is often limited by their lifetime and stability due to the limited number of pulses generated using explosive emission cathodes and the formation of unnecessary plasma on high-frequency metallic structures and output windows.[14] Furthermore, portrayal of device performance in terms of power density places a strong emphasis on average power production at higher frequencies. Extended interaction klystron (EIK) is one of the most competitive high-power generation devices in the family of vacuum electronic devices.[15–17] Due to the composition of multiple multi-gap cavities, the EIK has high circuit impedance and considerable output power and interaction efficiency.[18] Therefore, at high frequencies, it not only has a higher gain-bandwidth product than the traditional klystron, but also has a shorter total circuit length than the traveling wave tube (TWT).[19] Moreover, its compactness further reduces device weight and volume due to lower magnetic field requirements than gyrotrons. While the EIK holds great promise as a high-power source, there are still many challenges to be solved, which mainly share many of the

same plasma physics challenges faced by high-power microwave generators.[20] With the expansion of devices to millimeter wave and higher frequency bands, high-frequency structures will become extremely small due to the co-transition effect of device structure size and frequency. The compact size of high-frequency sources in principle requires that the electron beam must have tiny transverse dimensions and potentially very high current densities to maintain sufficiently high gain and power.[21] Therefore, current challenges about the micro-fabrication of interaction circuits are perhaps trumped by the difficulties in producing small diameter, high current, precisely-aligned electron beams. In addition, the strong electric field concentrated in the small cavity will inevitably increase the risk of breakdown and arcing, and affect the stable operation of the device.

With the increasing demand for high power in compact high frequency devices, insights gained using overmoded structures in fast-wave device development can be extended to linear beam devices typified by EIKs.[22] The power limitation imposed by cross-sectional dimensions which shrink with wavelength can be overcome by using cavities and waveguides that are much larger than the wavelength in transverse dimension due to operation in higher-order modes.[23] Currently, various high-order mode structures and innovative structures designed by combining multi-beam and sheet-beam have been widely studied.[24–30] Multi-beam technology and coaxial structure have been widely used in conventional high-power klystrons.[31] When maintaining the same current density as the traditional single beam, multiple beams can provide a larger total current for the high-frequency structure in a large cross-sectional area. However, in actual engineering implementation, it is difficult to completely format and limit the distributed arrangement of multiple beams within a short distance, and the output system is more complicated. The sheet beam spreads the total beam current over a wide cross-section, allowing significantly higher total electron beam current to be transported for a given voltage. Though employing the sheet beam is promising, its generation, focusing, and transport with narrow dimensions are still challenging.

In this paper, a tractable overmoded high frequency interaction circuit is presented. The operation mechanism of the quasi-TM_{02} in this interaction circuit is established, as shown in Fig. 1. Due to the Bessel function cross-sectional field strength distribution, the higher the order of the TM mode, the stronger the E_z-field strength around the central axis, and the greater the characteristic impedance.[32] By realizing the method of concentrating the axial field energy along the source's central axis within a large cavity, an oversized beam tunnel that can support efficient energy conversion between the intense electron beam and the high frequency field is designed. As shown in Fig.2, this overmoded structure has a far larger electron beam loading area than conventional structures.[33–35] In overmoded circuits, the mode competition is naturally enhanced in more oversized structures. Here, a trade-off analysis from introducing high order modes for achieving the larger circuit size to improving high order modes field distribution for maintaining sufficient electron-wave coupling and suppress mode competition is reported. Based on this quasi-TM_{02} mode structure, a six-cavity *Ka*-band EIK with a MW-level output power is thusly demonstrated.

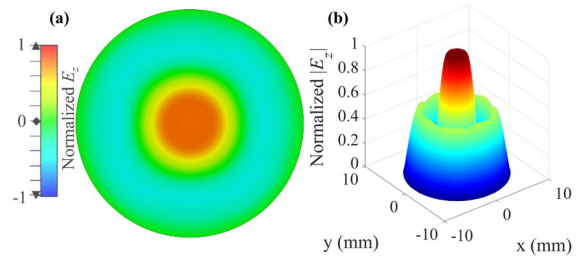

FIG. 1. (a) E_z-field distribution and (b) $|E_z|$-field contour plot of the quasi-TM_{02} mode at z = 0 plane.

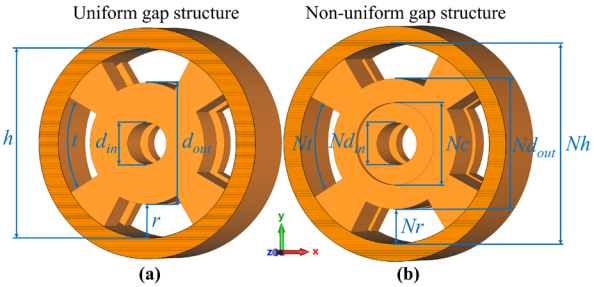

FIG. 2. Model dimensions for (a) uniform gap structure (UGS) and (b) non-uniform gap structure (NUGS).

II. DESIGN OF THE OVERMODED CIRCUIT

For conventional linear beam devices, as the interaction circuits become smaller as the frequency extends into the millimeter wave band, a smaller electron beam needs to be used to keep the beam diameter sufficiently smaller than the device operating wavelength. However, for a practical electron-optical system to be optimized for lifetime and electrical stresses, the current density emitted from the cathode must remain within a reasonable range, and the compression of the beam must be limited. Thus, the beam current is inevitably limited by the transverse size, which results in a significant reduction in output power. Here, enlarging the diameter of the beam tunnel to accommodate the high-current intense electron beam has become the technical key to solve the power limitation of millimeter-wave linear beam devices.

Compared with the commonly used fundamental mode, the most significant feature of the higher-order mode is that it can support a physically larger interaction system for a given frequency. From the Bessel function field of circular waveguide and cylindrical cavity resonator, the higher the TM mode order, the more concentrated the E_z-field strength in the axial central region. The concentration of the axial electric field not only improves the beam-wave interaction but also makes it possible to expand the diameter of the beam tunnel. After preliminary empirical analysis, the TM_{02}-based mode is selected. Figures 1(a) and 1(b) show the E_z-field distribution at the cross section of a single interaction gap. The established operating mode exhibits the strongest E_z-field distribution at and near the central axis, which enhances the interaction with the electron beam passing through the central axis. Combining the field distribution established by the axisymmetric circular

waveguide and the cylindrical cavity resonator, a novel disk-loaded structure with four coupled holes is proposed, as shown in Fig. 2(a). The four fan-shaped coupling holes are evenly distributed in axisymmetric manner. It is worth noting that the numerous geometric parameters of the disk-loaded structure with coupling holes provide a corresponding degree of flexibility for defining various technical indicators of the circuit and for the study of high frequency characteristics. The initial design parameters are listed in Table I. The beam tunnel diameter of the four-coupling-hole disk-loaded structure designed based on overmoded operation can easily be increased by three times or more than that of the conventional linear beam devices.[33–35] Even compared with the current promising coaxial multi-beam EIK,[28] the single tunnel size of this RSWS can still support an intense electron beam with a higher total current without requiring expensive and complex electron optical systems.

TABLE I
DESIGN PARAMETERS

Symbol	Description	Value and Unit
d_{in}	Beam tunnel diameter of UGS	3.60 mm
d_{out}	Center disk outer diameter of UGS	10.54 mm
r	Coupling hole radius of UGS	2.88 mm
t	Coupling hole angular width of UGS	60°
h	Entire cavity diameter of UGS	16.30 mm
Nd_{in}	Beam tunnel diameter of NUGS	3.60 mm
Nd_{out}	Center disk outer diameter of NUGS	11.10mm
Nc	Groove diameter of NUGS	7.00 mm
Nr	Coupling hole radius of NUGS	2.88 mm
Nt	Coupling hole angular width of NUGS	60°
Nh	Entire cavity diameter of NUGS	16.86 mm

III. CIRCUIT CHARACTERISTICS AND STABILITY ANALYSIS

The designed overmode structure provides a substantial solution to the size and power constraints of the device, but multimode coexistence and mode competition are naturally enhanced in more oversized high-frequency structures. All of these efforts are justified because the apparent increase in the transverse dimension of the high-frequency structures relative to the wavelength allows the application of denser electron beams, which will translate into further improvements in generation power. The crucial technique to suppress mode competition is to make the circuit establish a positive field between the electron beam and the desired mode to enhance the existence of the desired mode field, and a relatively negative field between the electron beam and the undesired mode to weaken the presence of the competing mode field. Beam-wave interaction theory of classical linear beam devices notes that the electron beam interacts with the E_z component of the electric field in the central region. Therefore, TM_{0n} modes preferably interact with the electron beam on the central axis, where the index n is determined by the variation in the distribution pattern of the axial electric field along the radial direction. Since the designed circuit is based on a finite period structure realized in a disk-loaded coupled cavity, a number of discrete frequencies are generated by the number of half-wavelengths between the cavity end walls. Typically, the greater the number of periods contained in each cavity, the more discrete modes there will be. To reduce the adverse effects caused by mode competition, we expect to use the two-gap structure to form the front input cavity and the middle buncher cavity of the designed EIK, and use the three-gap structure as the output cavity.

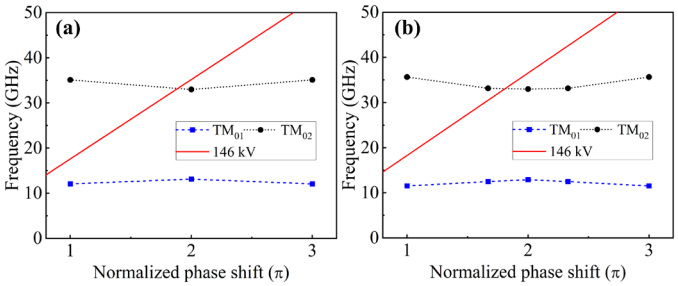

FIG. 3. Dispersion diagrams of (a) two-gap cavity and (b) three-gap cavity.

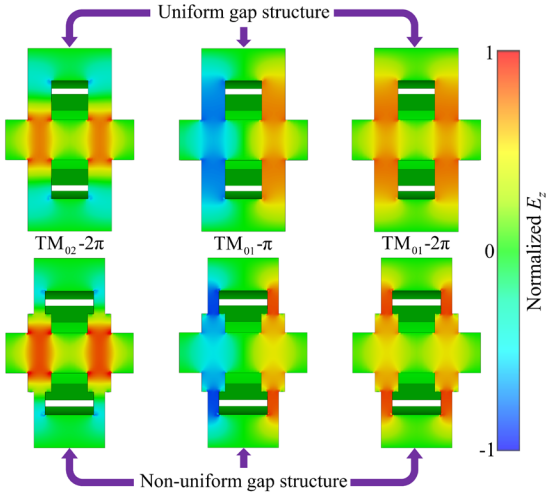

FIG. 4. The E_z-field magnitude distributions for the desired working mode and the undesired competing mode for the UGS and the NUGS.

The operating mode field characteristics of the four-coupling-hole disk-loaded structure are studied using commercially available 3D electromagnetic analysis software (CST Microwave Studio). Figures 3(a) and 3(b) show the dispersion characteristics of the two structures, respectively. The axial mode is planned as the 2π mode that provides an electric field in the same direction on each gap, which ensures the effective modulation of the electron beam. Due to the E_z-field distribution within the beam tunnel region of the interaction gap, discrete modes of TM_{01} are considered as potentially competing risks to the desired TM_{02} mode. To weaken the E_z-field strength of the TM_{01} mode at the center of the gap, we further propose an improved non-uniform gap structure (NUGS) based on the original uniform gap structure (UGS), as shown in Fig. 2(b). Figure 4 shows the E_z-field magnitude distributions for the desired working mode and the undesired competing mode for the UGS and the NUGS. The sudden change of the electric field intensity in the beam tunnel area caused by the non-uniformity of the gap width is related to the difference of the field distribution of the TM_{01} and TM_{02} modes in the cross section. Because the half-standing wave numbers of TM_{01} mode and TM_{02} mode distributed radially in

the gap are different, changing the width of the gap has the effect of adjusting the energy storage and thus changing the field distribution. As shown in Fig. 4, the E_z-field strength on and near the central axis of the TM_{02} mode is further enhanced by reducing the width of the outer edge portion of the gap. At the same time, the E_z-field strength of TM_{01} mode on and near the central axis is weakened. We further normalize the E_z-field amplitude of each mode field along the axial direction in the beam tunnel, as shown in Fig. 5. Through comparative analysis, the TM_{02} mode of the NUGS has the strongest E_z-field amplitude at and near the central axis compared with other modes.

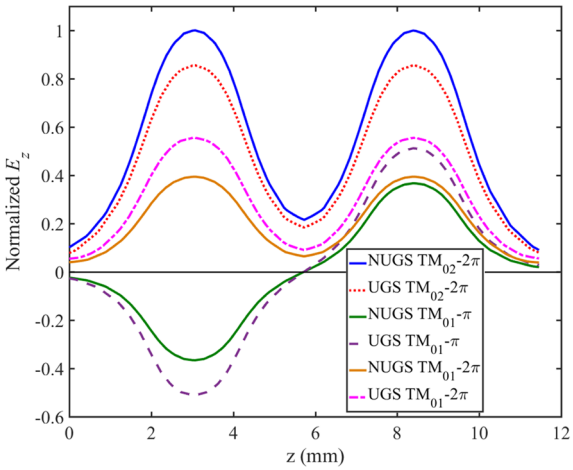

FIG. 5. The distribution of the E_z-field amplitude along the axial direction in the beam tunnel of each mode of the UGS and the NUGS.

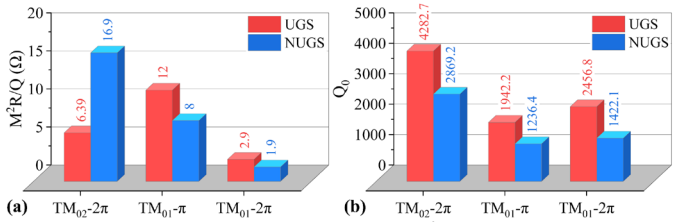

FIG. 6. (a) Effective characteristic impedance M^2R/Q and (b) intrinsic quality factor Q_0 of the UGS and the NUGS.

The different field distributions of these two structures also affect the high-frequency characteristic parameters. Coupling coefficient M and characteristic impedance R/Q of the resonant circuit are important indexes that capture the energy coupling between the high-frequency field and electron beam. The M and R/Q are given in the following equations,[36] respectively

$$\frac{R}{Q}=\frac{\left(\int\left|E_z\right|\cdot dl\right)^2}{2\omega W} \tag{1}$$

$$M\left(\beta_e\right)=\frac{\int_{-\infty}^{\infty}E\left(z\right)e^{j\beta_e z}dz}{\int_{-\infty}^{\infty}\left|E\left(z\right)\right|dz} \tag{2}$$

where ω is the angular frequency, W is the total stored energy, $E(z)$ is the longitudinal field distribution, β_e is the propagation constant of the electron beam. Generally, the effective characteristic impedance M^2R/Q is used to evaluate the beam-wave coupling performance.[37] The calculation results and comparative analysis of the effective characteristic impedance M^2R/Q of the UGS and the NUGS are shown in Fig. 6 (a). Due to the enhancement of the field strength in the beam tunnel region within the gap, the NUGS greatly increases the M^2R/Q value of the TM_{02} mode. Compared with the UGS, the NUGS can make the TM_{02} mold have the largest M^2R/Q, and also reduce the M^2R/Q of the TM_{01} competition mode. Field analysis for both structures is verified here, highlighting the advantage of the NUGS for suppressing low-order TM_{01} mode.

In the process of beam-wave interaction, not only the influence of the competition modes must be alerted, but also the self-oscillation of the operation mode should be kept in mind. Especially in the intermediate cavity of the EIK, the self-oscillation of the working mode or the oscillation of the undesired modes will perturb the electron bunching, so as to distort the normal signal amplification. Here, we carry out an extensive study on the beam-wave synchronization and oscillating starting conditions of the designed circuit so as to further suppress possible mode competition. The total quality factor Q_t is a common technical indicator for evaluating the self-oscillation of interacting circuits, expressed as[38]

$$\frac{1}{Q_t}=\frac{1}{Q_0}+\frac{1}{Q_e}+\frac{1}{Q_b} \tag{3}$$

where Q_0 and Q_e are the intrinsic quality factor and externally loaded quality factor, respectively. Q_b is beam-loaded quality factor, defined as[26]

$$\frac{1}{Q_b}=G_e\left(\frac{R}{Q}\right) \tag{4}$$

where G_e is the beam-load conductance. G_e is derived from the space-charge wave theory, expressed as[39, 40]

$$G_e=\frac{1}{8}\frac{\beta_e}{\beta_q}G_0\left[\left|M_-^2\left(\beta_e-\beta_q\right)\right|-\left|M_+^2\left(\beta_e+\beta_q\right)\right|\right] \tag{5}$$

where β_q is the propagation constants of the reduced plasma. G_0 is the DC conductance of the electron beam. $M_-\left(\beta_e-\beta_q\right)$ and $M_+\left(\beta_e+\beta_q\right)$ represent the coupling coefficients of fast and slow space charge waves. Actually, the fast and slow space charge waves are directly responsible for the modulation on electrons, making the RF signal gradually amplified. Generally, g_e is used to represent the ability to transfer energy from the electron beam to the circuit, where $g_e = G_e / G_0$. Negative g_e indicates that the DC energy of the electron beam is converted into high-frequency field energy, and this mode may be excited. Meantime, the larger the peak value of the negative g_e indicates that the mode field is more readily excited during oscillation. To maintain the stability of the oscillating circuit, it is necessary that the lossy conductive wall and the external load fully absorb the energy released by the electron beam. We usually consider that when $Q_t < 0$, the oscillating circuit will have a tendency to start oscillating. Here to avoid self-oscillation, $Q_t > 0$ is required. Q_e is infinite for an unloaded intermediate cavity, while Q_0 is related to the inner wall ohmic losses and is always positive. Therefore, Q_b should also be as positive as possible. At this time, $g_e > 0$ is required in the appropriate beam voltage range. Figures

7(a) and 7(b) show the change of the g_e with the electron beam DC voltage for these two structures, respectively. Through the analysis of the beam-wave synchronization conditions, when the operating voltage is set between 100 kV and 150 kV, the resonant modes near the beamline will not have the tendency of self-oscillation.

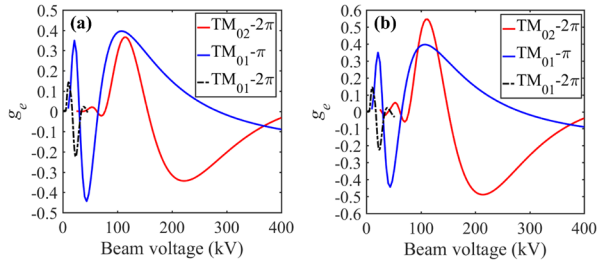

FIG. 7. The g_e of the (a) UGS and the (b) NUGS as a function of the electron beam voltage.

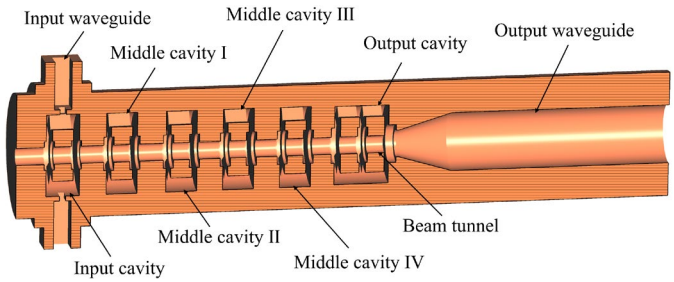

FIG. 8. Schematic diagram of a six-cavity *Ka*-band extended interaction klystron (EIK).

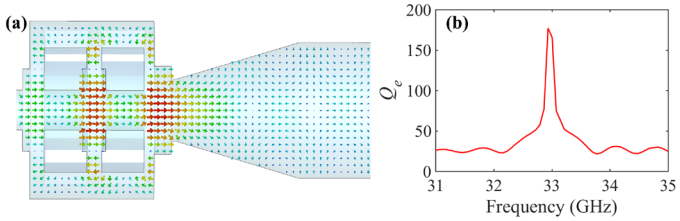

FIG. 9. (a) Simulated electric field distribution on the longitudinal section of the output cavity. (b) The Q_e of output circuit calculated by group delay.

Based on the four-coupling-hole disk-loaded structure, a *Ka*-band EIK consisting of an input cavity, four middle cavities, and an output cavity has been designed, as shown in Fig. 8. Another important advantage of this overmode structure compared with the conventional ladder-type interaction circuit is that the maximum axial field energy of the TM_{02} mode can be directly coupled to the output waveguide through aperture diffraction. The condition for coupling between the main and secondary resonators or waveguides through the small aperture is that the normal component of the electric field or the tangential component of the magnetic field in the same direction exist in the main and secondary resonators or waveguides at the same time, and these components cannot be zero at the same time at the position of the small aperture. Since the TM_{02} mode has a normal electric field perpendicular to the common wall, through a small hole opened on the central axis of the end of the cavity, the electric field lines will pass through the small hole and excite the TM_{01} mode field in the output waveguide to propagate, as shown in Fig. 9(a). Here we use the group delay time method to solve the diffraction quality factor of the output cavity.[41] The Q_e obtained by the group delay time is 176.7 at 32.94 GHz, as shown in Fig. 9(b). Table II lists the physical parameters of each cavity, where f is the resonant frequency, p is the period length.

TABLE II
PARAMETERS OF EACH CAVITY

Cavity	f (GHz)	p (mm)	$M^2(R/Q)$ (Ω)	Q_t
Input Cavity	32.90	5.56	39.8	68
Middle Cavity I	32.84	5.36	16.6	1279
Middle Cavity II	32.89	5.36	16.7	1277
Middle Cavity III	32.93	5.36	16.8	1274
Middle Cavity IV	32.98	5.36	16.9	1271
Output Cavity	32.92	5.16	16.9	177

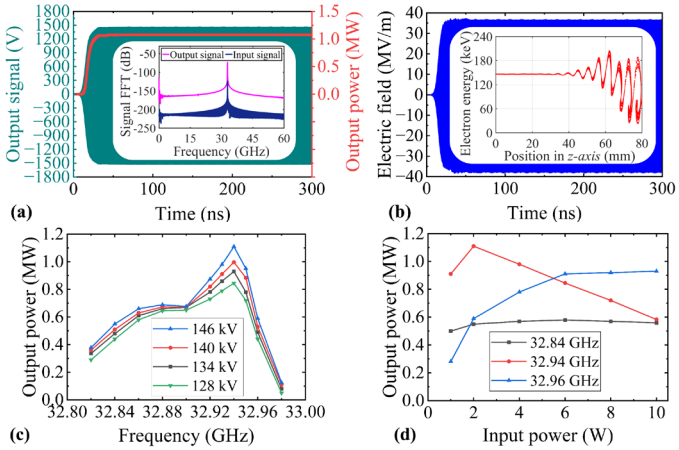

FIG. 10. (a) Output signal power. Inset: Frequency spectrums of the input and output signals. (b) Amplitude at the gap in the output cavity where the electric field is strongest. Inset: Phase-space diagram of electron energy. (c) Output power as a function of input signal sweep frequency characteristics. (d) Output power as a function of input power.

IV. PARTICLE-IN-CELL (PIC) SIMULATION

To verify the stability and beam-wave interaction capability of the overmoded circuit, 3-D particle-in-cell (PIC) simulations are carried out for the EIK by using the CST. Since the EIK only requires single-beam operation and has an oversized beam tunnel, a conventional Pierce electron gun can be used to drive this highly overmoded circuit, and a uniform permanent magnet system can be used to maintain the focus of the electron beam.[42] Assuming pulsed operation, an electron beam with a diameter of 3.3 mm and a current of 24 A is injected into the high-frequency circuit at a bias of 146 kV. A constant magnetic field of 0.55 T is used to focus the electron beam. To get closer to reality, we use reduced effective conductivity values to replace the extra ohmic losses caused by surface roughness. The conductivity of the cavity wall is set to 3.6×10^7 S/m, corresponding to a surface roughness of 0.15 μm, which is about 62% of the ideal conductivity of oxygen-free copper. The input cavity adopts a dual-port structure, one port is connected to the excitation signal source, and the other port is connected to the matched load, so as to improve the working bandwidth. The standard WR-28 waveguide is applied to the input cavity. Figure 10(a) shows the output signal, output power and its spectrum when the input power is 2 W at 32.94 GHz. A

maximum output power of 1.11 MW is obtained at 32.94 GHz in the circular waveguide TM_{01} mode, with a corresponding gain and efficiency of 57 dB and 31.7%, respectively. As shown in Fig. 10(b), the maximum field strength of the cavity is 38.12 MV/m, which is less than the vacuum breakdown field strength. The inset of Fig. 10(b) shows the modulation and bunching when the electron beam interacts with the operating mode. Fig. 10(c) shows the output power as a function of the input signal sweep-frequency characteristics when the input power is 2 W. The 3-dB bandwidth reaches 120 MHz, from 32.84 to 32.96 GHz. Fig. 11(d) shows the effect of input power on output performance. The closer to the edge of the operating band, especially at the high frequency end, the more power is required to drive this EIK into saturation.

V. CONCLUSION

The substantial increase in the output power of conventional linear beam devices has proven a significant and ongoing technical challenge. In order to realize the high-current electron beam loading capability of compact devices, an overmoded interaction circuit with a larger beam tunnel size than conventional structures is designed. Even compared to the promising multi-beam and sheet-beam structures, its single tunnel can still support an intense electron beam with a high total current without the need for complex electron optical system and focusing system. Through the optimized analysis of high-frequency characteristics, the four-coupling-hole disk-loaded interaction circuit operating in TM_2 mode shows worthwhile potential in overcoming the output power limitations, improving the beam-wave coupling ability and operating stability. A MW-class *Ka*-Band EIK operating stably in the TM_{02} mode based on this structure has been verified by 3-D PIC simulation. Such new design approaches are expected to be used to develop coherent electromagnetic radiation sources with higher frequency, higher power and higher efficiency.

ACKNOWLEDGMENTS

This work was supported in part by the National Key Research and Development Program of China under Grant 2019YFA0210202, in part by National Natural Science Foundation of China under Grant 61771096, and in part by Sichuan Science and Technology Program under Grant 2021YJ0096.

DATA AVAILABILITY

The data that support the findings of this study are available from the corresponding author upon reasonable request.

REFERENCES

[1] Y. Gong, Q. Zhou, M. Hu, Y. Zhang, X. Li, H. Gong, J. Wang, D. Liu, Y. Liu, Z. Duan, and J. Feng, "Some advances in theory and experiment of high-frequency vacuum electron devices in China," IEEE Trans. Plasma Sci. **47**(5), 1971–1990 (2019).

[2] N. C. Luhmann, Jr., H. Bindslev, H. Park, J. Sanchez, G. Taylor, and C. X. Yu, "Microwave diagnostics," Fusion Sci. Technol. **53**(2), 335–396 (2008).

[3] L. Krier, I. G. Pagonakis, K. A. Avramidis, G. Gantenbein, S. Illy, J. Jelonnek, J. Jin, H. P. Laqua, A. Marek, D. Moseev, and M. Thumm, "Theoretical investigation on possible operation of a 140 GHz 1 MW gyrotron at 175 GHz for CTS plasma diagnostics at W7-X," Phys. Plasmas **27**(11), 113107 (2020).

[4] V. L. Granatstein, R. K. Parker, and C. M. Armstrong, "Vacuum electronics at the dawn of the twenty-first century," Proc. IEEE **87**(5) 702–716 (1999).

[5] J. Benford, J. A. Swegle, and E. Schamiloglu, *High Power Microwaves*, 3rd ed. (Taylor & Francis, New York, 2016).

[6] A. Mase, Y. Kogi, D. Kuwahara, Y. Nagayama, N. Ito, T. Maruyama, H. Ikezi, X. Wang, M. Inutake, T. Tokuzawa, J. Kohagura, M. Yoshikawa, S. Shinohara, A. Suzuki, F. Sakai, M. Yamashika, B. J. Tobias, C. Muscatello, X. Ren, M. Chen, C. W. Domier, and N. C. Luhmann, "Development and application of radar reflectometer using micro to infrared waves," Adv. Phys.-X **3**(1), 633–675 (2018).

[7] D. K. Abe, J. P. Calame, C. D. Joye, A. M. Cook, J. Pasour, S. Cooke, A. N. Vlasov, I. A. Chernyavskiy, B. Levush, K. T. Nguyen, D. E. Pershing, D. Chernin, "Millimeter-wave and sub-millimeter-wave vacuum electronics amplifier development at the US Naval Research Laboratory," Proc. SPIE **8624**, 86240H (2013).

[8] L. J. R. Nix, L. Zhang, W. He, C. R. Donaldson, K. Ronald, A. W. Cross, and C. G. Whyte, "Demonstration of efficient beam-wave interaction for a MW-level 48 GHz gyroklystron amplifier," Phys. Plasmas **27**(5), 053101 (2020).

[9] R. Bingham, J. Mendonca, P. Shukla, "Plasma based charged-particle accelerators," Plasma Phys. Control. Fusion **46**(1), 1–23 (2004).

[10] M. D. Abouzahra and R. K. Avent, "The 100-kW millimeter-wave radar at the Kwajalein atoll," IEEE Antennas Propag. Mag. **36**(2) 7-19 (1994).

[11] A. A. Tolkachev, B. A. Levitan, G. K. Solovjev, V. V. Veytsel and V. E. Farber, "A megawatt power millimeter-wave phased-array radar," IEEE Aerosp. Electron. Syst. Mag. **15**(7), 25-31 (2000).

[12] T. C. Luce, "Applications of high-power millimeter waves in fusion energy research," IEEE Trans. Plasma Sci. **30**(3), 734-754 (2002).

[13] S. H. Gold and G. S. Nosinovich, "Review of high-power microwave source research," Rev. Sci. Instrum. **68**(11), 3945–3974 (1997).

[14] J. Zhang, D. Zhang, Y. Fan, J. He, X. Ge, X. Zhang, J. Ju, and T. Xun, "Progress in narrowband high-power microwave sources," Phys. Plasmas **27**(1), 010501 (2020).

[15] D. Berry, H. Deng, R. Dobbs, P. Horoyski, M. Hyttinen, A. Kingsmill, R. MacHattie, A. Roitman, E. Sokol, and B. Steer, "Practical aspects of EIK technology," IEEE Trans. Electron Devices **61**(6), 1830–1835 (2014).

[16] B. Steer, A. Roitman, P. Horoyski, M. Hyttinen, R. Dobbs, and D. Berry, "Millimeter-wave extended interaction klystrons for high power ground, airborne and space radars," *in Proceedings of 41st European Microwave Conference*, Manchester, 2011, pp. 984–987.

[17] J. Zhao, H. Yin, L. Zhang, L. W. He, Q. Zhang, A. D. R. Phelps, and A. W. Cross, "Experiments on W-band extended interaction oscillators with pseudospark sourced post-accelerated electron beam," Phys. Plasmas **24**(6), 060703 (2017).

[18] D. H. Preist and W. J. Leidigh, "Experiments with high-power CW Klystrons using extended interaction catchers," IEEE Trans. Electron Devices **10**(3), 201–211 (1963).

[19] J. Luo, J. Feng, and Y. Gong, "A review of microwave vacuum devices in China: Theory and device development including high-power klystrons, spaceborne TWTs, and gyro-TWTs," IEEE Microw. Mag. **22**(4), 18–33 (2021).

[20] J. H. Booske, "Plasma physics and related challenges of millimeter-wave-to-terahertz and high power microwave generation," Phys. Plasmas, **15**(5), 055502 (2008).

[21] J. H. Booske, R. J. Dobbs, C. D. Joye, C. L. Kory, G. R. Neil, G. S. Park, J. Park, and R. J. Temkin, "Vacuum electronic high power terahertz sources," IEEE Trans. Terahertz Sci. Technol. **1**(1), 54-75 (2011).

[22] R. K. Parker, R. H. Abrams, B. G. Danly, and B. Levush, "Vacuum electronics," IEEE Trans. Microw. Theory Techn. **50**(3), 835–845 (2002).

[23] L. Bi, L. Meng, Y. Yin, C. Xu, S. Zhu, R. Peng, F. Zeng, Z. Chang, B. Wang, H. Li, and P. Zhang, "Power enhancement for millimeter-wave extended interaction radiation sources by using the TM_{31}-mode scheme," Phys. Plasmas **26**(6), 063101 (2019).

[24] D. Wang, G. Wang, J. Wang, S. Li, P. Zeng, and Y. Teng, "A high-order mode extended interaction klystron at 0.34 THz," Phys. Plasmas **24**(2), 023106 (2017).

[25] J. Li, Z. Wu, M. Hu, R. Zhong, K. Zhang, J. Zhou, D. Liu, and S. Liu, "Research on optimized structure of a 220-GHz extended interaction oscillator," Phys. Plasmas **28**(9), 093108 (2021).

[26] J. Qing, X. Niu, T. Zhang, Y. Liu, G. Guo, and H. Li, "THz radiation from a TM_{51} mode sheet beam extended interaction oscillator with low injection," IEEE Trans. Plasma Sci. **50**(4) 1081–1086 (2022).

[27] S. Lü, C. Zhang, S. Wang, and Y. Wang, "Stability analysis of a planar multiple-beam circuit for *W*-band high-power extended-interaction klystron," IEEE Trans. Electron Devices **62**(9), 3042–3048 (2015).

[28] X. Zhang, R. Zhang, and Y. Wang, "Study of a dual-mode multibeam interaction circuit with coaxial structure for *Ka*-band high-power EIK," IEEE Trans. Electron Devices **68**(2), 822–828 (2021).

[29] X. Li, Z. Wu, Y. Luo, S. Liao, J. Wang, J. Gao, Z. Liu, Y. Wan, L. Rui, Y. Wang, G. Liu, and W. Jiang, "High-efficiency study of an SBEIO based on the SAA optimization," IEEE Trans. Electron Devices **66**(11), 4938–4942 (2019).

[30] J. Pasour, K. Nguyen, E. Wright, A. Balkcum, J. Atkinson, M. Cusick, and B. Levush, "Demonstration of a 100-kW solenoidally focused sheet electron beam for millimeter-wave amplifiers," IEEE Trans. Electron Devices **58**(6) 1792–1797 (2011).

[31] J. C. Cai, I. Syratchev, and G. Burt, "Design study of a high-power *Ka*-band high-order-mode multibeam klystron" IEEE Trans. Electron Devices **67**(12), 5736–5742 (2020).

[32] D. M. Pozar, *Microwave Engineering*, 4th ed. New York, NY, USA: Wiley, 2011.

[33] D. Zhao, W. Gu, X. Hou, G. Liu, Q. Xue, and Z. Zhang, "Demonstration of a high-power *Ka*-band extended interaction klystron," IEEE Trans. Electron Devices **67**(9), 3788–3794 (2020).

[34] H. Gong, Y. Gong, T. Tang, J. Xu, and W.-X. Wang, "Experimental investigation of a high-power Ka-band folded waveguide traveling-wave tube," IEEE Trans. Electron Devices **58**(7) 2159–2163 (2011).

[35] C. Paoloni, M. Mineo, M. Henry, and P. G. Huggard, "Double corrugated waveguide for Ka-band traveling wave tube," IEEE Trans. Electron Devices **62**(11), 3851–3856 (2015).

[36] C. Xu, B. Wang, R. Peng, L. Bi, F. Zeng, Z. Chang, S. Zhu, Y. Yin, H. Li, and L. Meng, "Start current study of a THz sheet beam extended interaction oscillator," Phys. Plasmas **25**(7), 073103 (2018).

[37] N. Guo, Z. Qu, X. Shang, H. Ding, K. Liu, W. Song, H. Wang, J. Wang, D. Zhao, and Q. Xue, "Analysis and improvement of performance instability in extended interaction klystrons with random geometrical perturbations," IEEE Trans. Electron Devices **69**(10), 5886–5894 (2022).

[38] X. Xu, X. Yuan, H. Li, Q. Chen, Y. Zu, M. Cole, J. Xie, Y. Yin, and Y. Yan, "Design of a G-band extended interaction klystron based on a three-coupling-hole structure," IEEE Trans. Electron Devices, **69**(3), 1368–1373 (2022).

[39] S. Li, J. Wang, G. Wang, and D. Wang, "Theoretical studies on stability and feasibility of 0.34 THz EIK," Phys. Plasmas **24**(5), 053107 (2017).

[40] M. Chodorow and T. Wessel-Berg, "A high-efficiency klystron with distributed interaction," IRE Trans. Electron Devices **8**(1), 44–55 (1961).

[41] Y. Ding, *Theory and Computer Simulation of High Power Klystron*. Beijing, China: National Defense Industry Press, 2008, pp. 44–47.

[42] A. S. Gilmour, and I. Ebrary, *Klystrons, traveling wave tubes, magnetrons, crossed-field amplifiers, and gyrotrons.* Norwood, US: Artech HouseBooks, 2011.